Chemical Engineering Journal 198-199 (2012) 364–370

Contents lists available at SciVerse ScienceDirect

Chemical Engineering Journal

journal homepage: www.elsevier.com/locate/cej

An emulsion phase condensation model to describe the defluidization behavior for reactions involving gas-volume reduction

Yue Chu, Bozhao Chu, Xiaobo Wei, Qiang Zhang *, Fei Wei *

Beijing Key Laboratory of Green Chemical Reaction Engineering and Technology, Department of Chemical Engineering, Tsinghua University, Beijing 100084, China

HIGHLIGHTS

- An emulsion phase condensation model to describe the fluidization of reactions involving a gas volume decrease.
- Onion-shaped distributions of reactant concentration and gas velocity in the emulsion phase.
- The minimum gas velocity, emulsion phase voidage and the fluidization quality are predicted.
- The prediction of the fluidization quality and the fluidization diagram fit well with the published experiment results.

GRAPHICAL ABSTRACT

A phase diagram for fluidization quality in fluidized-bed reactor with reactions involving gas volume reduction carried on is provided by the phase condensation model. The solid line refers to conditions in which the minimum gas velocity in the emulsion phase equals u_{mf}. The left side region of the line indicate stable operation conditions while in the above region of the line, poor fluidization even defluidization may occur. Four kinds of fluidization phenomena are observed at different operation parameters in experiments. The experiment results are in good accord with division of operation regions by simulation results, showing the credibility and good prediction of the emulsion phase condensation model.

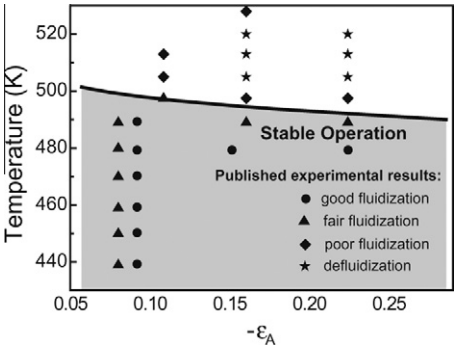

ARTICLE INFO

Article history:
Received 27 March 2012
Received in revised form 25 May 2012
Accepted 1 June 2012
Available online 13 June 2012

Keywords:
Fluidization
Phase condensation model
Gas-volume reduction
Emulsion phase
Simulation

ABSTRACT

The fluidization quality decreases drastically when the reactions involving a gas volume decrease were carried out in a fluidized bed reactor. The model to describe the defluidization behavior for reactions involving gas-volume reduction is highly required to choose proper operation parameters. Herein a phase condensation model is proposed to describe the fluidization and the transfer behavior of the chemical reactions involving a gas volume decrease when they are carried out in a fluidized bed reactor. The phase condensation model concerns an emulsion phase domain. The mass transfer between bubbles and the modeling domain, the governing equations for the hydrodynamics and mass transport, the Brinkman equation, together with the kinetic sub-model are incorporated in the model. The simulation result captures the spatial distribution of reactant concentration and gas velocity which is onion-shaped for the CO_2 hydrogenation reaction. The fluidization quality can be predicted by the phase condensation model. The result indicates that lower temperature and higher inert gas content in the feed gas are favorable for good fluidization. A phase diagram of fluidization quality is obtained using temperature and expansion factor as indices. The phase condensation model renders the precise prediction which compares well with published experimental data.

* Corresponding authors. Fax: +86 10 6277 2051.
E-mail addresses: zhang-qiang@mails.tsinghua.edu.cn (Q. Zhang), wf-dce@tsinghua.edu.cn (F. Wei).

1385-8947/$ - see front matter © 2012 Elsevier B.V. All rights reserved.
http://dx.doi.org/10.1016/j.cej.2012.06.001

Nomenclature

c	concentration of CO_2, mol/m^3
c_{A0}	initial concentration of CO_2, mol/m^3
De	effective diffusion coefficient, m^2/s
E	effective activation energy, kJ/mol
$\boldsymbol{F}$	volume force, N/m^3
g	acceleration due to gravity, m/s^2
ΔH_{H2}	effective enthalpy of H_2 adsorption, kJ/mol
ΔH_{CO2}	effective enthalpy of CO_2 adsorption, kJ/mol
ΔH_{H2O}	effective enthalpy of H_2O adsorption, kJ/mol
H	distance to the reactor inlet, m
$\boldsymbol{I}$	unit column vector, $[11]^T$, dimensionless
K_{be}	phase transfer coefficient, m/s
k_a	kinetic rate constant, mol/kg/s/kPa$^{-5/6}$
K_{H2}	equilibrium constant of H_2, kPa$^{-1/2}$
K_{CO2}	equilibrium constant of CO_2, kPa$^{-1/2}$
K_{H2O}	equilibrium constant of H_2O, kPa^{-1}
p	pressure, Pa
P_0	inlet pressure, Pa
P_t	outlet pressure, Pa
R	reaction rate, mol/(m^3 s)
R_g	gas constant (=8.314 J/mol K)
T	temperature, K
$\boldsymbol{u}$	gas velocity, m/s
u	r-velocity, m/s
u_{mf}	minimum fluidization velocity, m/s
u_t	terminal velocity, m/s
v	z-velocity of $\boldsymbol{u}$, m/s
x_A	conversion of CO_2, dimensionless
y_{A0}	initial molar ratio of CO_2

Greek letters

α	initial ratio of H_2 to CO_2, dimensionless
δ_A	expansion per mole of CO_2, dimensionless
ε_A	expansion factor, (=$y_{A0}\ \delta_A$), dimensionless
ε_p	emulsion phase voidage, dimensionless
$\varepsilon_{p\,mb}$	ε_p at minimum bubbling fluidization
$\varepsilon_{p\,mf}$	ε_p at minimum fluidization
η	dynamic viscosity, Pa s
η_g	ratio of gas volume at $x_A = x_A$ to $x_A = 0$, dimensionless
$\eta_{g\,min}$	ratio of gas volume at $x_A = 1$ to $x_A = 0$, dimensionless
κ	permeability, m^2
κ_{dv}	dilatational viscosity, Pa s
ρ	gas density, kg/m^3
ρ_0	initial gas density, kg/m^3
ρ_P	bulk density of the particle, kg/m^3

1. Introduction

The fluidized bed reactors have a broad range of applications from metallurgical roasting to coal conversion, petroleum refinery, agricultural, food, pharmaceutical, and material processes [1–7]. The fluidization of catalyst particles leads to superior transfer and hydrodynamic characteristics which are important for reactions with significant thermal effect and involving catalyst regeneration. For the reactions involving a gas volume decrease carried out in a fluidized bed reactor, the fluidization quality decreases drastically leading to a sharp change in the reactor temperature and catalyst entrainment, which induces poor-quality products and safety issue of the fluidized reactor [8–10]. Such phenomena have been observed in industrial reactor for gas phase reactions, such as polymerization [11,12], hydrogenation [13–17], hydrochlorination [18,19], methanol synthesis [13,20], Fischer–Tropsch synthesis [21–24], and NO reduction by CO [25]. Some process developments were ended in failure attributed from this aspect. For instance, the fluidized-bed Fischer–Tropsch synthesis, which had planned to produce liquid hydrocarbons for gasoline from natural gas via CO and H_2 using a fluidized bed reactor initially investigated in Brownsville (TX, USA) in the later 1940s. However, the poor fluidization quality attributed from the volume decrease reaction inhibits their scale up [22–24].

A family of researches have been carried out to investigate these phenomena and tried to overcome this problem. Abba et al. firstly pointed out the possibility of defluidization as a consequence of volume reduction through modeling of the variable-density fluidized bed reactor [26]. Kai et al. carried out a series of excellent experimental investigations for CO_2 hydrogenation in a fluidized catalyst bed [27–30]. They directly observed the slugging defluidization occurring in the bed using glass reactors. A fluidization diagram using the composition of feed gas and the reaction rate constant as the two indices to illustrate a stable operation region was provided. A significant decrease in the emulsion-phase voidage was measured by the bed-collapse method when the defluidization occurred. The mechanism of such kind of phenomena was proposed and generally approved that the incomplete compensation of gas transported from the bubble to the emulsion phase for gas reduction caused by reaction leading to condensation of emulsion phase and defluidization.

As the hot model experiments are time-consuming, both the modeling and simulation have attracted considerable research effort to obtain proper operation parameters for experiments [31–34]. Up to now, the models to describe the effect of volume change on conversion in fluidized bed reactor have been reported [26,35–43]. These models were based on the classical two-phase model, while the mechanism of defluidization was little explored. The whole reactor was chosen as the modeling domain, therefore, the detailed hydrodynamic information is missing. A mathematic model to investigate the influence of volume change on the hydrodynamic behavior is still lacking.

This work aims to develop a mathematic model named as the phase condensation model to investigate the hydrodynamic as well as the transfer behavior in a fluidized bed for reactions involving a gas volume decrease based on the mechanism of defluidization. Different with the previous models in which the whole reactor was considered, an emulsion phase domain surrounded by bubbles is chosen as the modeling domain in the current emulsion phase condensation model. The reason is that the hydrodynamic behavior of the emulsion phase domain plays a decisive role in the fluidization of the whole bed for reactions involving gas-volume reduction. The mass transfer between the bubble and emulsion phase is also considered. In the modeling emulsion phase domain, the conservations of momentum and mass as well as a kinetic submodel are conducted. The CO_2 hydrogenation is chose as the typical case for the reason that the hydrodynamic behavior (including the defluidization) of CO_2 hydrogenation have been well investigated by Kai et al. [27,28,44] when it was operated in a fluidized bed reactor. The simulation result provides detailed information (e.g. the concentration and velocity distribution) of the emulsion phase. The fluidization behavior is predicted at different operating conditions. The phase diagram to indicate the fluidization quality and defluidization zone is established based on simulation results.

The simulation results were compared with the experimental results published by Kai et al. [27] to validate the predication of the phase condensation model.

2. Mathematical model and numerical simulations

To describe the hydrodynamic behavior in the emulsion phase, a columniform part of the emulsion phase surrounded by bubbles located in the bottom of the fluidized bed is chosen as the investigation domain. The parameters of the fluidized bed employed in the current research are identical with those used in the experimental investigation reported by Kai et al. [27]. The length and inner diameter of the bed are 1.5 m and 50 mm, respectively. 450 g catalyst particles were introduced into the fluidized bed reactor. The settled bed height is 0.4 m and the ratio between the fixed bed height and the column diameter is 8.0. The superficial gas velocity is 50 mm/s. Table 1 lists the governing equations for describing the hydrodynamic behavior in the emulsion phase. The gas phase movement is modeled by the momentum conservation equation. The CO_2 hydrogenation reaction involves significant gas volume reduction, the density of gas is not fixed. Therefore, a weakly compressible Navier–Stokes equation (N–S equation) is employed in the current research. In the emulsion phase, the gas flows through a porous bed which is made up of catalyst particles. The Brinkman equation is used to describe the flow in porous domain. The bed permeability is calculated based on the formula by Lei et al. [45]. The changeable gas density ρ is determined by the CO_2 conversion involving gas volume reduction, as shown in Eq. (5). The conversion can be related to concentration of CO_2, the variable in this model (shown in Eq. (6)). So the gas density is obtained using an expression with the CO_2 concentration (c) as the variable shown in the following equations:

$$\rho = \frac{\rho_0}{1 + \varepsilon_A x_A} \tag{5}$$

$$\frac{c}{c_{A0}} = \frac{1 - x_A}{1 + \varepsilon_A x_A} \tag{6}$$

$$\rho = \rho_0 \frac{1 + \varepsilon_A c/c_{A0}}{1 + \varepsilon_A} \tag{7}$$

Table 1
The governing equations in the model.

Governing equations for gas phase flow
Conservation equation of momentum
$\rho(\mathbf{u}\cdot\nabla)\mathbf{u} = \nabla\cdot[-p\mathbf{I} + \eta(\nabla\mathbf{u} + (\nabla\mathbf{u})^{T}) - (2\eta/3 - \kappa_{dv}) \times (\nabla\cdot\mathbf{u})\mathbf{I}] + \mathbf{F}$ (1)
Brinkman equation
$\nabla\cdot\left[-\frac{\mu}{\varepsilon_P}(\nabla\mathbf{u} + (\nabla\mathbf{u})^{T}) + p\mathbf{I}\right] = -\frac{\eta}{\kappa}\mathbf{u}$ (2)
Continuity equation
$\nabla\cdot(\rho\mathbf{u}) = 0$ (3)
Conservation equation of mass
$\nabla\cdot(D_e\nabla c) = R - \mathbf{u}\cdot\nabla c$ (4)

Table 2
The kinetic constants for hydrogenation of CO_2 model on the 20 wt.% Ni–10 wt.% La_2O_3/γ-Al_2O_3 catalyst.

k_a (mol/kg/s/kPa$^{-5/6}$)	K_{H_2} (kPa$^{-1/2}$)	K_{CO_2} (kPa$^{-1/2}$)	K_{H_2O} (kPa^{-1})
9.32×10^3	3.77×10^{-11}	1.43×10^{-4}	2.75×10^{-8}
E (kJ/mol)	ΔH_{H_2} (kJ mol)	ΔH_{CO_2} (kJ mol)	ΔH_{H_2O} (kJ mol)
72.5	−90.2	−29.5	−64.3

The gas transport in the emulsion phase is modeled by the mass conservation equation. The convection–diffusion equation (c–d equation) is employed as the mass-balance equation. The effective diffusion coefficient involved in the equation is defined as the product porosity and the molecular diffusion coefficient. As the catalysts used in CO_2 hydrogenation reaction are classified as "AA group", the fluidization style in emulsion phase belongs to the particulate fluidization region [44]. Therefore, the Richardson–Zaki law proposed by Richardson and Zaki [46] is used to calculate the voidage of the emulsion phase. The reaction rate is provided from the kinetic sub-model.

2.1. The kinetic sub-model to describe the hydrogenation of CO_2 process

The selectivity of methane is almost 100% in the CO_2 hydrogenation process. Thus, the following main reaction is considered in the present kinetic model with the kinetic parameters achieved and validated in a fixed bed microreactor (see Table 2) [47].

$$CO_2 + 4H_2 = CH_4 + 2H_2O$$

$$r = -\frac{kP_{H_2}^{1/2}P_{CO_2}^{1/3}}{(1 + K_{H_2}P_{H_2}^{1/2} + K_{CO_2}P_{CO_2}^{1/2} + K_{H_2O}P_{H_2O})^2} \tag{8}$$

The temperature influence of the rate and equilibrium constants in the above equation are described by the Arrhenius equations:

$$k = k_a \exp(-E/R_gT) \tag{9}$$

$$K = K_a \exp(-\Delta H/R_gT) \tag{10}$$

2.2. The numerical method and computational conditions

The solution to the above model has been successfully incorporated with the Comsol Multiphysics 3.5 software. The proven finite element method (FEM) is used to solve the models.

An axial symmetry cylinder of emulsion phase is considered in the model. The modeling domain is reduced to a 2D geometry with rotational symmetry with a width of 1.5 cm and a height of 1.5 cm (Fig. 1). The size of the modeling domain is determined from the bubble size, the gas holdup ratio, together with the size of experimental reactor. The mesh for this domain is 60 (W) × 60 (H). The computational conditions and the additional parameters are given in Table 3. The physical properties (such as the density and viscosity of the gas mixture) are determined through weighted average based on the molar composition. The heat transfer in the domain is not considered, that is, uniform temperature distribution is assumed in the modeling domain under different operating temperatures. As some parameters are sensitive to temperature and gas composition, their values listed in Table 3 are determined at 483 K with the molar ratio of hydrogen to CO_2 at a stoichiometric value. The boundary conditions for the domain boundaries (Fig. 1) are listed as follows:

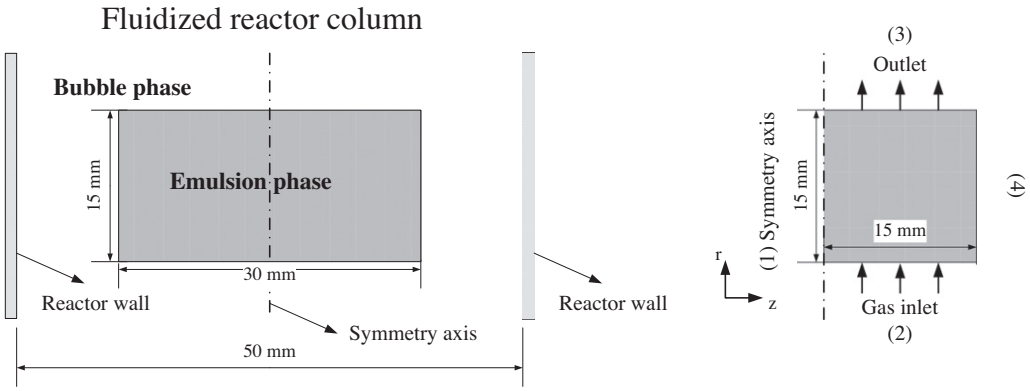

Fig. 1. Schematic geometry of the simulated 2D emulsion phase domain.

Table 3
The computation conditions and additional parameters.

Parameter	Value	Parameter	Value
Particle parameters		Temperature (K)	483
Mean diameter (μm)	55	Pressure (kPa)	100
Bulk density (kg/m^3)	600	N–S equation parameters	
Physical properties of gas		Constant in Richardson–Zaki law	4.65
Inlet density (kg/m^3)	0.10	Permeability (m^2)	2.95×10^{-12}
Viscosity of CO_2 (kg/m/s)	1.37×10^{-5}	*c–d* equation parameters	
Viscosity of H_2 (kg/m/s)	8.42×10^{-6}	Molecular diffusion coefficient (m^2/s)	1.02×10^{-4}
Operating conditions at inlet		Phase transfer coefficient (m/s)	12.2

(1) the axial symmetry;

(2) the pressure inlet boundary condition for N–S equation, $P = P_0$; the flux boundary condition for *c–d* equation, the flux through the boundary equals the amount of gas transport from the bubble to the emulsion phase shown in Eq. (11);
(3) the pressure outlet boundary condition for N–S equation, $P = P_t$, P_t is calculated as Eq. (12); the flux boundary condition for *c–d* equation;
(4) the velocity outlet boundary condition for N–S equation, $u = 0$, no restriction for v; flux boundary condition for *c–d* equation. The mass transfer coefficient between bubble phase and emulsion phase is calculated with the formula from Zahram and Tafreshi's publication [38].

$$K_{be}(c_{A0} - c) = -De\nabla c + cv \tag{11}$$

$$P_t = P_0 - [\rho_P(1 - \varepsilon_P) + \rho\varepsilon_P]gH \tag{12}$$

3. Result and discussion

3.1. The spatial distribution of concentration in the emulsion phase

Fig. 2 shows the spatial distribution of reactant concentration in the modeling emulsion phase domain. The simulation result is obtained under good fluidization condition. A typical operating parameter for good fluidization is chosen as follows: the temperature is 483 K, the CO_2 content is 4.76% in the feed gas. The molar ratio of H_2/CO_2 is 20, indicating the hydrogen is five times excessive as the stoichiometric ratio of H_2/CO_2 is 4. The large amount of hydrogen is to weaken the effect of gas volume reduction caused by chemical reaction. The effect of feed gas composition on the fluidization quality is studied in Section 3.3.

As shown in Fig. 2, the left line of this square is the rotational symmetrical axis, and the total distribution of the cylinder is an onion-like distribution: a high reactant concentration appears in the outside part, while the concentration becomes lower in the central part. The difference is caused by the mass transport between the bubble phase and the emulsion phase. In the assumption of the two-phase model of bubbling fluidized bed proposed by Toomey and Johnstone [48], the reactions only take place in the emulsion phase, and the consumed reactant is compensated by the bubbles. Another assumption in two-phase model is that the flow style of emulsion phase can be treated as a mixed flow or a plug

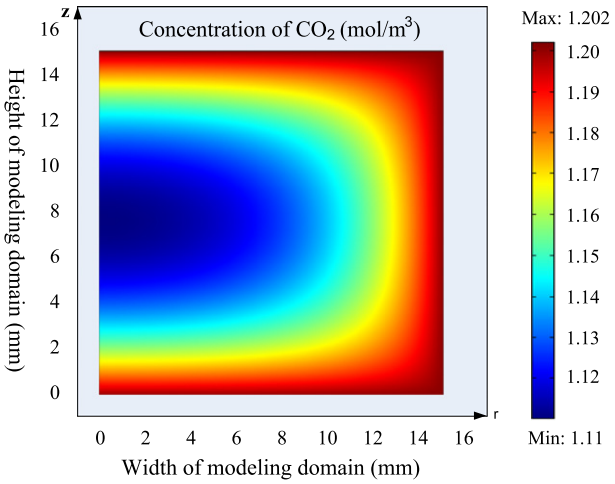

Fig. 2. The spatial distribution of CO_2 concentration in the modeling domain (Temperature: 483 K, The molar content of CO_2 in feed gas: 4.76%, H_2/CO_2 in feed gas: 20, The inlet pressure: 100 kPa).

flow. While the simulation results showed that the flow style are actually much more complex.

3.2. The distribution of gas velocity in the emulsion phase

The distribution of gas velocity in the modeling emulsion phase at 483 K with a content of 4.76% CO_2 in feed gas is illustrated as Fig. 3. The whole distribution of velocity is similar to that of concentration shown in Fig 2. The gas velocity is higher in the outside part and lower in the central part. There is the minimum gas velocity at the central of the modeling domain, where is the middle of the symmetry axis (boundary (1) as shown in Fig. 1). The effect of reaction involving gas volume reduction on gas flow can be observed. The calculated minimum fluidization velocity (u_{mf}) is 1.238 mm/s, which is close to the gas velocity in the emulsion phase. If the reaction rate increases at higher temperature, the gas velocity becomes smaller than u_{mf}. The gas drag force is too small to balance the gravitation and buoyancy force [49]. Therefore, the agglomeration firstly appears in the central part of the emulsion phase, and the defluidized region becomes larger, leading to channeling or slugging phenomena [50,51].

3.3. The prediction of gas velocity and voidage in the emulsion phase

For reactions involving gas volume reduction, gas volume contraction caused by consumption of reaction can be expressed as:

$$\eta_g = 1 + \varepsilon_A x_A \tag{13}$$

The parameter η_g is the relative gas volume at conversion x_A based on the initial gas volume. ε_A is the expansion factor defined as:

$$\varepsilon_A = y_{A0}\delta_A \tag{14}$$

where δ_A is the balance between the sums of the stoichiometric coefficients of products and reactants. The value of δ_A is -2 for the hydrogenation of CO_2 reaction. As the defluidization is caused by the imbalance of gas consumed in the emulsion phase and gas compensated from the bubble phase, such phenomenon can be avoided by controlling the gas volume reduction content to an adequate level. From the Eq. (13), it can be seen that both the conversion x_A and the content of CO_2 in feed gas y_{A0} are key factors. Furthermore, the reaction temperature plays an important role in conversion. As a result, the temperature and y_{A0} are the main operating indices affecting fluidization quality obviously.

In the experiments of lab scale and industrial operating, it is observed that the defluidization of a small region in the fluidized bed extends to the adjacent region when the reaction involving gas volume reduction operated in it, leading to defluidization of large area [23,27,28,44]. Therefore, we focus on the minimum gas velocity in the modeling emulsion phase domain. The minimum gas velocity in the emulsion phase which is located in the center of the modeling domain has been well discussed in section 3.2. The minimum gas velocity is predicted at different temperatures and feed gas compositions using the phase condensation model (Fig. 4), where α is defined as the molar ratio of H_2 to CO_2 in the feed gas and the fluidization number is calculated by gas velocity divided by the minimum fluidization velocity (v/u_{mf}).

The gas velocity decreases with temperature increases at different feed gas compositions. This is attributed from the temperature is the index of reaction rate and the phase exchange coefficient. At higher temperature, the gas consuming rate becomes faster as well as the gas exchange between the bubble and the modeling domain. While the simulation results show that the increase of the gas consuming rate is faster than that of gas exchange, so the gas velocity decreases. Such phenomenon has been observed experimentally by Kai et al. [27]. They noted that the fluidization quality began to decrease around 483 K in case of $\alpha = 7.8$, and then the defluidization occurred at 503 K. From the $\alpha = 8$ curve in Fig. 4, similar operating parameters are presented. The gas velocity equals to the minimum fluidization velocity (u_{mf}) at approximately 500 K. When the operating temperature is higher than 500 K, the gas velocity becomes lower than u_{mf}. As a result, the drag force is too small to balance the gravitation and buoyancy force leading to defluidization. The effect of temperature on the fluidization quality at $\alpha = 8$ drawn from simulation results is almost the same to the published experimental results in reference [27]. The comparison of the experimental and the simulation result indicates the good credibility of phase condensation model.

The relationship between the gas velocity and feed gas composition is also apparent. The molar content of CO_2 in feed gas y_{A0} directly affects the gas volume contraction. To obtain lower content of CO_2, the inert gas or excess H_2 is introduced into the feed gas. The latter method is widely used. As shown in Fig 4, the minimum gas velocity in emulsion phase becomes larger for higher ratio of H_2 to CO_2 under the same inlet gas velocity. Another interesting point (Fig. 4) lies in the difference of reactor temperatures when the minimum gas velocity equals u_{mf}. When H_2 in feed gas is twice excessive ($\alpha = 8$), the highest operating temperature to obtain stable fluidization is 492 K. While if H_2 in feed gas is 8 times excessive

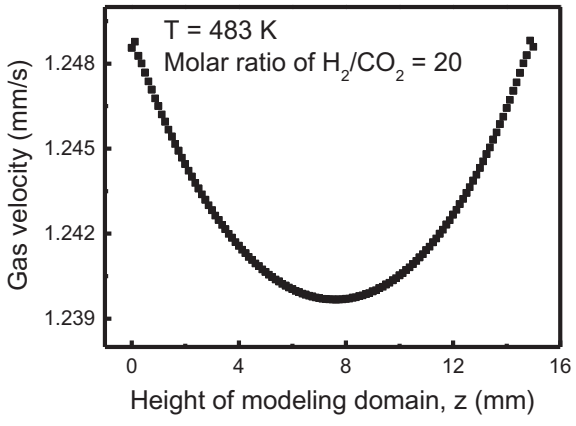

Fig. 3. The variation of gas velocity with height along the rotation symmetry axis in the modeling domain (Temperature: 483 K, The molar content of CO_2 in feed gas: 4.76%, H_2/CO_2 in feed gas: 20, The inlet pressure: 100 kPa).

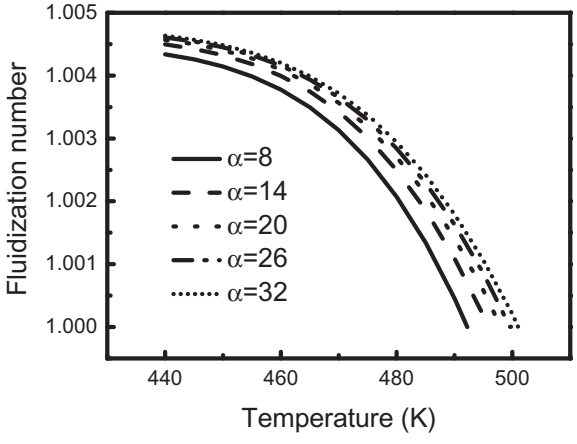

Fig. 4. The prediction of the minimum gas velocity located in the center of the modeling domain with different feed gas compositions. (α is the molar ratio of H_2 to CO_2 in the feed gas).

Table 4
The maximum CO_2 conversion (x_A) at different temperatures and gas compositions in the modeling domain.

α	8	14	20	26	32
T (K)	492	496	498	500	501
x_A (%)	6.77	11.80	16.60	21.80	26.30

($\alpha = 32$), a good fluidization quality is obtained at 501 K. This phenomenon has been observed in experiments by Kai et al. [27,30]. Table 4 shows the maximum CO_2 conversion at different conditions. When H_2 in feed gas is 8 times excessive, the conversion is 4 times that of hydrogen twice excessive, but as the limit of gas volume contraction is small ($\eta_{g\min} = 93.9\%$), a good fluidization quality is available. If a high conversion is needed for an industrial production, the content of the other reactant in feed gas is increased and the fluidization quality can be improved simultaneously in this case.

The variation of the minimum emulsion phase voidage with temperature under different feed gas compositions is illustrated as Fig. 5. The Richardson–Zaki law is used to calculate the voidage of the emulsion phase (shown in the following equation):

$$\varepsilon_P = \sqrt[4.65]{\frac{v}{u_t}} \tag{15}$$

The changing trend of emulsion phase voidage is similar to that of gas velocity. The voidage decreases when the temperature increases or the H_2/CO_2 ratio decreases. The effect of temperature and feed gas composition on the emulsion phase voidage has been experimentally investigated by Kai et al. by a bed-collapse method [27]. In their experiments, the H_2/CO_2 ratio (α) was fixed to be 7.8. An apparent emulsion phase condensation was observed when the temperature is higher than 473 K and that the emulsion phase voidage decreases gradually with the increase of temperature. The experimental phenomenon exhibits the same trend with the simulation result at $\alpha = 8$ (Fig. 5). When the H_2/CO_2 ratio (α) is changed from 7.8 to 34 at 513 K, they observed that the emulsion phase voidage decreased with α decreasing. Such phenomenon can also be clearly found in the simulation results shown in Fig. 5.

It is generally accepted that for bubbling fluidization at good fluidization quality, minimum fluidization is kept in the emulsion phase and rest inlet gas forms bubbles. While as the particles used in this research are classified as "AA group" which are easily aerated, the voidage is slightly higher than $\varepsilon_{p\,mf}$ which is the emulsion phase voidage at minimum fluidization. The minimum voidage in

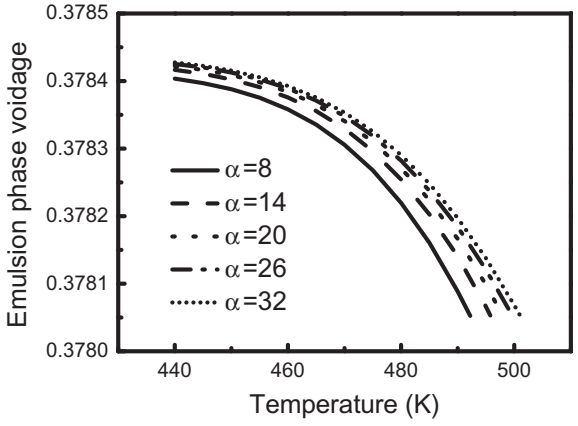

Fig. 5. The variation of the minimum emulsion phase voidage located in the center of the modeling domain with temperature at different feed gas compositions (α is the molar ratio of H_2 to CO_2 in the feed gas).

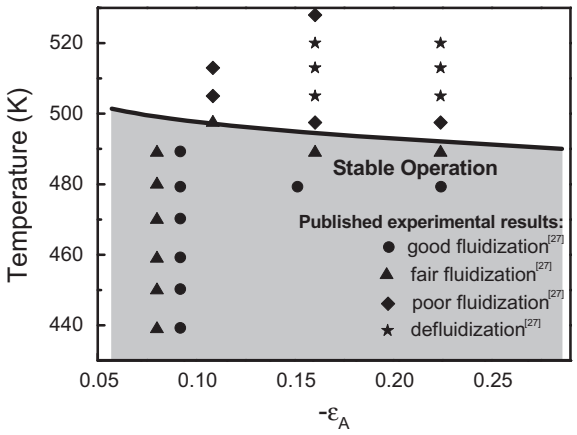

Fig. 6. The fluidization diagram based on two indices (The symbols are the published experiment results [27]; the line represents the modeling results, the left side region of the line represents the stable fluidization region, the right side of the line represents the poor fluidization even defluidization region).

the emulsion phase is close to $\varepsilon_{p\,mf}$. When the gas volume contraction caused by reaction consumption is distinct, the emulsion phase condensation is apparent and its voidage may become lower than $\varepsilon_{p\,mf}$ indicating that defluidization occurs. Therefore, the extent of emulsion phase condensation is a direct indication for the fluidization quality and the emulsion phase voidage can be used as the indicator, that's why our model is named that way.

3.4. The phase diagram of fluidization quality

A fluidization diagram is proposed based on the prediction of minimum gas velocity (Fig. 4) and the minimum voidage (Fig. 5) in the emulsion phase with both the temperature and the expansion factor ε_A as indices (Fig. 6). This diagram provides instructions to choose proper operation parameters to avoid defluidization. The solid line represents parameters at which the minimum gas velocity in the emulsion phase equals u_{mf} (the fluidization number equals 1 in Fig. 4), furthermore the minimum voidage in the emulsion phase equals $\varepsilon_{p\,mf}$. When the fluidized bed is operated at the solid line, a minimum fluidization is achieved in the emulsion phase. On the left-side region of the line, the emulsion phase further expands and its voidage is higher than $\varepsilon_{p\,mf}$. While on the right-side region, apparent emulsion phase condensation occurs and the emulsion phase voidage is lower than $\varepsilon_{p\,mf}$. This indicated that the stable fluidization operation is possible when the operating parameters are in the left-side region of the line (Fig. 6). While if the reaction conditions correspond to the area above the line in the figure, a poor fluidization quality may occur. The figure shows that defluidization occurred when the temperature exceeds 495 K and the ratio of H_2 to CO_2 in feed gas is below 12 ($-\varepsilon_A > 0.15$). This operation region should be avoided to obtain stable fluidization in a fluidized bed for a volume reduction reaction.

The experiment results published by Kai et al. [27] are also listed on Fig 6 by solid symbols. Four kinds of fluidization quality, from good fluidization to defluidization, are observed at different operation parameters in experiments by Kai et al. [27]. The experimental results at different operation conditions are located in the corresponding region of diagram drawn from simulation results perfectly, showing the good validation of the emulsion phase condensation model.

4. Conclusions

An emulsion phase condensation model is developed to describe the hydrodynamic and transfer behavior for reactions

involving a gas volume decrease. The fluidization quality in the fluidized-bed reactor was also predicted. The simulation results provide a feature of spatial distribution of reactant concentration and the gas velocity in the modeling emulsion phase domain. The distribution has an onion-like shape with the lowest gas velocity existing in the central part. It is predicted that a good fluidization quality requires a relatively low temperature and more inert gas in feed flow. A large content of excessive hydrogen in feed gas allows high temperature operation for high conversion of CO_2 hydrogeneration. A fluidization diagram is available with simulation data using the two indices. The simulation results fit well with published experimental results. It serves as the guide to choose proper operation parameters to avoid defluidization in the fluidized-bed reactors. This phase condensation model provides a new path for the simulation of fluidization and transfer behavior for reactions involving gas volume reduction operated in fluidized-bed reactor. By changing the kinetic sub-model and other additional parameters, the phase condensation model can be used in other reactions involving gas volume decrease. Therefore, a modeling platform for hydrodynamic behavior for a variable-gas-density fluidized bed reactor was provided.

Acknowledgements

The work was supported by the Foundation for the Natural Scientific Foundation of China (No. 20736004), the China National Program (No. 2011CB932602), Research Fund for the Doctoral Program of Higher Education of China (No. 20100002110022).

References

[1] P. Basu, Combustion of coal in circulating fluidized-bed boilers: a review, Chem. Eng. Sci. 54 (1999) 5547–5557.
[2] J. Corella, J.M. Toledo, G. Molina, A review on dual fluidized-bed biomass gasifiers, Ind. Eng. Chem. Res. 46 (2007) 6831–6839.
[3] R.C. Ellis, X. Li, J.B. Riggs, Modeling and optimization of a model IV fluidized catalytic cracking unit, AIChE J. 44 (1998) 2068–2079.
[4] Y. Chen, H. Zhou, J. Zhu, Q. Zhang, Y. Wang, D. Wang, F. Wei, Direct synthesis of a fluidizable SAPO-34 catalyst for a fluidized dimethyl ether-to-olefins process, Catal. Lett. 124 (2008) 297–303.
[5] Q. Zhang, M.Q. Zhao, J.Q. Huang, J.Q. Nie, F. Wei, Mass production of aligned carbon nanotube arrays by fluidized bed catalytic chemical vapor deposition, Carbon 48 (2010) 1196–1209.
[6] M.Q. Zhao, Q. Zhang, J.Q. Huang, J.Q. Nie, F. Wei, Layered double hydroxides as catalysts for the efficient growth of high quality single-walled carbon nanotubes in a fluidized bed reactor, Carbon 48 (2010) 3260–3270.
[7] Q. Zhang, J.Q. Huang, M.Q. Zhao, W.Z. Qian, F. Wei, Carbon nanotube mass production: principles and processes, ChemSusChem 4 (2011) 864–889.
[8] G. Tardos, R. Pfeffer, Chemical-reaction induced agglomeration and defluidization of fluidized-beds, Powder Technol. 85 (1995) 29–35.
[9] A. Reichhold, B. Kronberger, G. Friedl, Temporary defluidization in fine powder fluidized beds caused by changing the fluidizing gas, Chem. Eng. Sci. 61 (2006) 2428–2436.
[10] S. Jašo, H. Arellano-Garcia, G. Wozny, Oxidative coupling of methane in a fluidized bed reactor: Influence of feeding policy, hydrodynamics, and reactor geometry, Chem. Eng. J. 171 (2011) 255–271.
[11] H. Hatzantonis, H. Yiannoulakis, A. Yiagopoulos, C. Kiparissides, Recent developments in modeling gas-phase catalyzed olefin polymerization fluidized-bed reactors: the effect of bubble size variation on the reactor's performance, Chem. Eng. Sci. 55 (2000) 3237–3259.
[12] A. Leach, F. Portoghese, C. Briens, F. Berruti, A new and rapid method for the evaluation of the liquid-solid contact resulting from liquid injection into a fluidized bed, Powder Technol. 184 (2008) 44–51.
[13] Q. Zhang, Y.Z. Zuo, M.H. Han, J.F. Wang, Y. Jin, F. Wei, Long carbon nanotubes intercrossed Cu/Zn/Al/Zr catalyst for CO/CO_2 hydrogenation to methanol/dimethyl ether, Catal. Today 150 (2010) 55–60.
[14] S.G. Diao, W.Z. Qian, G.H. Luo, F. Wei, Y. Wang, Gaseous catalytic hydrogenation of nitrobenzene to aniline in a two-stage fluidized bed reactor, Appl. Catal. A 286 (2005) 30–35.
[15] J.H. Wang, Z.L. Yuan, R.F. Nie, Z.Y. Hou, X.M. Zheng, Hydrogenation of nitrobenzene to aniline over silica gel supported nickel catalysts, Ind. Eng. Chem. Res. 49 (2010) 4664–4669.
[16] W.J. Lee, C.Z. Li, Catalytic reactions of ethylene and hydrogen in a fluidized-bed reactor with ni nanoparticles, Energy Fuel. 23 (2009) 4866–4870.
[17] J.S. Kim, S. Lee, S.B. Lee, M.J. Choi, K.W. Lee, Performance of catalytic reactors for the hydrogenation of CO_2 to hydrocarbons, Catal. Today 115 (2006) 228–234.
[18] X.B. Wei, H.B. Shi, W.Z. Qian, G.H. Luo, Y. Jin, F. Wei, Gas-phase catalytic hydrochlorination of acetylene in a two-stage fluidized-bed reactor, Ind. Eng. Chem. Res. 48 (2009) 128–133.
[19] H.Y. Zhang, B. Dai, X.G. Wang, L.L. Xu, M.Y. Zhu, Hydrochlorination of acetylene to vinyl chloride monomer over bimetallic Au–La/SAC catalysts, J. Ind. Eng. Chem. 18 (2012) 49–54.
[20] G.G. Wang, Y.Z. Zuo, M.H. Han, J.F. Wang, Cu–Zr–Zn catalysts for methanol synthesis in a fluidized bed reactor, Appl. Catal. A 394 (2011) 281–286.
[21] S.H. Kang, J.W. Bae, J.Y. Cheon, Y.J. Lee, K.S. Ha, K.W. Jun, D.H. Lee, B.W. Kim, Catalytic performance on iron-based Fischer–Tropsch catalyst in fixed-bed and bubbling fluidized-bed reactor, Appl. Catal. B 103 (2011) 169–180.
[22] B.H. Davis, Overview of reactors for liquid phase Fischer–Tropsch synthesis, Catal. Today 71 (2002) 249–300.
[23] T. Knowlton, S. Karri, A. Issangya, Scale-up of fluidized-bed hydrodynamics, Powder Technol. 150 (2005) 72–77.
[24] B.H. Davis, Fischer–Tropsch synthesis: overview of reactor development and future potentialities, Top. Catal. 32 (2005) 143–168.
[25] J. Li, G.H. Luo, Y. Chu, F. Wei, Experimental and modeling analysis of NO reduction by CO for a FCC regeneration process, Chem. Eng. J. 184 (2012) 168–175.
[26] I.A. Abba, J.R. Grace, H.T. Bi, Variable-gas-density fluidized bed reactor model for catalytic processes, Chem. Eng. Sci. 57 (2002) 4797–4807.
[27] T. Kai, K. Toriyama, K. Nishie, T. Takahashi, M. Nakajima, Effect of volume decrease on fluidization quality of fluidized catalyst beds, AIChE J. 52 (2006) 3210–3215.
[28] T. Kai, T. Takahashi, Formation of particle agglomerates after switching fluidizing gases, AIChE J. 43 (1997) 357–362.
[29] T. Kai, M. Furukawa, T. Nakazato, T. Tsutsui, K. Mizuta, M. Nakajima, Analysis of fluidization quality of a fluidized bed with staged gas feed for reactions involving gas-volume reduction, AIChE J. 56 (2010) 2297–2303.
[30] T. Kai, M. Furukawa, T. Nakazato, M. Nakajima, Prevention of defluidization by gas dilution for reactions involving gas-volume reduction, Chem. Eng. J. 166 (2011) 1126–1131.
[31] Y. Cheng, Y.C. Guo, F. Wei, Y. Jin, W.Y. Lin, Modeling the hydrodynamics of downer reactors based on kinetic theory, Chem. Eng. Sci. 54 (1999) 2019–2027.
[32] H.P. Zhu, Z.Y. Zhou, R.Y. Yang, A.B. Yu, Discrete particle simulation of particulate systems: a review of major applications and findings, Chem. Eng. Sci. 63 (2008) 5728–5770.
[33] B.L. Hou, H.Z. Li, Q.S. Zhu, Relationship between flow structure and mass transfer in fast fluidized bed, Chem. Eng. J. 163 (2010) 108–118.
[34] Z.S. Shi, W. Wang, J.H. Li, A bubble-based EMMS model for gas-solid bubbling fluidization, Chem. Eng. Sci. 66 (2011) 5541–5555.
[35] R.K. Irani, B. Kulkarni, L. Doraiswamy, Analysis of fluid bed reactors for reactions involving a change in volume, Ind. Eng. Chem. Fund. 19 (1980) 424–428.
[36] C.Y. Shiau, C.J. Lin, Analysis of volume change effects in a fluidized bed catalytic reactor, J. Chem. Technol. Biot. 56 (1993) 295–303.
[37] A. Adris, C. Lim, J. Grace, The fluidized-bed membrane reactor for steam methane reforming: model verification and parametric study, Chem. Eng. Sci. 52 (1997) 1609–1622.
[38] Z.M. Tafreshi, K. Opoku-Gyamfi, A.A. Adesina, A two-phase model for variable-density fluidized bed reactors with generalized nonlinear kinetics, Can. J. Chem. Eng. 78 (2000) 815–826.
[39] C.N. Wu, B.H. Yan, Y. Jin, Y. Cheng, Modeling and simulation of chemically reacting flows in gas-solid catalytic and non-catalytic processes, Particuology 8 (2010) 525–530.
[40] T. Kai, K. Nishie, T. Takahashi, M. Nakajima, Effects of decrease in gas volume due to reactions on the fluidization quality in a fluidized catalyst bed, Kagaku Kogaku Ronbun 30 (2004) 256–261.
[41] T. Kai, K. Toriyama, T. Takahashi, M. Nakajima, Defluidization caused by the reaction involving a volume reduction in a fluidized catalyst bed and improvement of the fluidity by internals, Kagaku Kogaku Ronbun 34 (2008) 351–357.
[42] A.S. Ibrehem, M.A. Hussain, N.M. Ghasem, Modified mathematical model for gas phase olefin polymerization in fluidized-bed catalytic reactor, Chem. Eng. J. 149 (2009) 353–362.
[43] I. Guedea, L.I. Díez, J. Pallarés, L.M. Romeo, Influence of O_2/CO_2 mixtures on the fluid-dynamics of an oxy-fired fluidized bed reactor, Chem. Eng. J. 178 (2011) 129–137.
[44] T. Kai, T. Tsutsui, S. Furusaki, Features of fluidized catalyst beds for proper design and operation of catalytic reactions, Ind. Eng. Chem. Res. 43 (2004) 5474–5482.
[45] S.Y. Lei, L.Q. Wang, L.Q. Jia, C.M. Xia, Relationship between porosity and permeability of the particles packed bed, J. Tsinghua Univ. 38 (1998) 76–79.
[46] J.F. Richardson, M. Zaki, Sediment Fluid: Part I, Trans. Inst. Chem. Eng. 32 (1954) 35–53.
[47] T. Kai, T. Takahashi, S. Furusaki, Kinetics of the methanation of carbon dioxide over a supported $Ni–La_2O_3$ catalyst, Can. J. Chem. Eng. 66 (1988) 343–347.
[48] R. Toomey, H. Johnstone, Gaseous fluidization of solid particles, Chem. Eng. Prog 48 (1952) 220–226.
[49] J. Siegell, High-temperature de fluidization, Powder Technol. 38 (1984) 13–22.
[50] D. Geldart, N. Harnby, A. Wong, Fluidization of cohesive powders, Powder Technol. 37 (1984) 25–37.
[51] H. Bi, J. Grace, Flow regime diagrams for gas-solid fluidization and upward transport, Int. J. Multiphas. Flow 21 (1995) 1229–1236.